



HAL
open science

RGD-functionalized magnetosomes are efficient tumor radioenhancers for X-rays and protons

Maha Hafsi, Sandra Preveral, Christopher Hoog, Joël Héroult, Géraldine Adryancyk Perrier, Christopher T. Lefèvre, Hervé Michel, David Pignol, Jérôme Doyen, Thierry Pourcher, et al.

► To cite this version:

Maha Hafsi, Sandra Preveral, Christopher Hoog, Joël Héroult, Géraldine Adryancyk Perrier, et al.. RGD-functionalized magnetosomes are efficient tumor radioenhancers for X-rays and protons. *Nanomedicine: Nanotechnology, Biology and Medicine*, 2020, 23, pp.102084. 10.1016/j.nano.2019.102084 . cea-02460533

HAL Id: cea-02460533

<https://cea.hal.science/cea-02460533>

Submitted on 3 Feb 2020

HAL is a multi-disciplinary open access archive for the deposit and dissemination of scientific research documents, whether they are published or not. The documents may come from teaching and research institutions in France or abroad, or from public or private research centers.

L'archive ouverte pluridisciplinaire **HAL**, est destinée au dépôt et à la diffusion de documents scientifiques de niveau recherche, publiés ou non, émanant des établissements d'enseignement et de recherche français ou étrangers, des laboratoires publics ou privés.

Magnetosomes are efficient tumor radioenhancers to both X-rays and protons

Maha Hafsi ^a, Sandra Preveral ^b, Christopher Hoog ^c, Joel Hérault ^d, Géraldine Adryanczyk Perrier ^b, Christopher T Lefèvre ^b, David Pignol ^b, Thierry Pourcher ^a, Jérôme Doyen ^d, Olivier Humbert ^a, Juliette Thariat ^{c,d,e} and Béatrice Cambien ^a.

^a Laboratoire TIRO, UMRE 4320, BIAM, DRT, CEA, Université de Nice-Sophia Antipolis, France.

^b Laboratoire de Bioénergétique Cellulaire, Institute of Biosciences and Biotechnologies of Aix Marseille (BIAM), UMR7265 CEA – CNRS - Aix Marseille Univ, CEA Cadarache, F-13108 Saint-Paul-lez-Durance, France

^c Department of Radiology, Centre Antoine Lacassagne, Nice, France.

^d Department of Radiation Therapy, Proton Therapy Center, Centre Antoine Lacassagne, Nice, France

^e Department of Radiation Oncology, Centre François Baclesse, Université de Normandie, France.

ABSTRACT :

Rationale

Radiation therapy is widely used for cancer treatment but its efficacy is limited by radioresistance and by damages caused to adjacent normal tissues. Active research aims at maximizing tumor eradication while reducing side-effects with theranostic nanoparticles that act as radioenhancers *in situ*. Ferromagnetic materials have been identified as promising nanotools for image-guided radiotherapy. Here, we investigated the potential of RGD-tagged magnetosomes (magnetosomes@RGD), bacterial biogenic magnetic nanoparticles naturally coated by a biological membrane and genetically engineered to express a RGD peptide, as tumour enhancers to conventional radiotherapy and proton therapy.

Methods

The potential of native and RGD-functionalized magnetosomes to enhance the effects of ionizing radiations was assessed in a DNA fragmentation assay and in melanoma and colorectal cancer cells using *in vitro* clonogenic assays. The *in vivo* radiotherapy enhancement efficacy of the magnetosomes@RGD was explored in preclinical models of melanoma-bearing mice treated with either X-rays or protons.

Results

Native and RGD-tagged magnetosomes similarly enhanced radiation-induced DNA damage. On cancer cells, both magnetoprobes were able to boost the killing efficacy of radiotherapy, although to a much larger extent with the magnetosomes@RGD enhancing the mortality by 2.5 fold in melanoma cells and by 2.9 fold in colorectal cancer cells. *In vivo* treatment of melanoma-bearing mice with magnetosomes@RGD prior to X-rays led to a 65% reduction in tumor development compared to radiotherapy alone (31%). Comparatively, a more effective tumor

growth inhibition (77%) was observed in combining RGD-decorated nanoprobe to proton therapy. The radioenhancing potential of magnetosomes@RGD was further evidenced by the DNA damage observed in the nanoscale vicinity of magnetosomes within the treated lesions.

Conclusions

Our results show efficacy of magnetosomes functionalized with a RGD peptide as tumor radioenhancers to both X-rays and protons *in vivo* and strengthen the interest of developing biogenic magnetoparticles for multimodal nanomedicine for cancer therapy.

Keywords: RGD functionalized magnetosome, biogenic iron-oxide nanoparticle, radiotherapy, proton therapy, cancer, radiosensitization, radioenhancement, magnetotactic bacteria

INTRODUCTION

Up to 50% of cancer patients receive radiotherapy (RT) at some time in their disease evolution (1). Although ionizing radiation dose is often needed to effectively kill tumor cells, dose delivery is limited by the severe damages caused to adjacent normal tissues. RT efficacy is also hampered by hypoxia-associated radiation resistance and other mechanisms of radioresistance that require that more dose be delivered to the tumor to achieve curability. Systemic radiosensitizing agents given concomitantly with radiation increase its local anti-tumor efficacy. However, such combination is associated with an increase of toxic, and sometimes limiting, systemic effects. With the development of nanotechnology, dose enhancement strategies have been proposed to improve radiation responses of tumours while minimizing side-effects. Very recently, such nanomedicine strategies have translated from bench to bedside and radioenhancing approaches are currently under investigation in a series of clinical trials (2,3).

To be an efficient radio-enhancer, the nano-object has to contain high-Z elements such as gold, gadolinium, platinum, iron, which under irradiation will generate secondary radiation and electrons at the subcellular scale. Radiation enhancement by scattered photons, photoelectrons, Compton and Auger electrons, etc (4,5) thus occurs by an increase of the dose deposited locally. Radiopaque radiation-effect enhancing nanoparticles can be used to image drug biodistribution in tissues (6). One drawback of such agents resides in their limited spatial selectivity. Among radiation-effect enhancing nanoparticles, iron oxide materials combine unique physicochemical (magnetic) properties for safe real-time MRI imaging and highly effective radioenhancement (7-9). However, passive targeting is available for certain tumours only and does not necessarily guarantee internalization of radiation-effect enhancing nanoparticles by targeted cells. Thus, iron-oxide based nano-objects have to be modified with suitable targeting ligands, such as small organic molecules, peptides, proteins, antibodies, and aptamers, to enable active cell targeting.

This has been done with variable success (10,11) due to the lack of solubility of iron-oxide nanoprobes in biological fluids. Indeed, modifications of surface characteristics are required to provide high dispersion stability (12). Moreover, coating strategies are still limited by the complex surface chemistry of the nano-probes, by relatively low receptor density on tumors and by homotypic and heterotypic binding properties of membrane receptors on cancer cells. The use of magnetosomes, biomineralized iron-oxide nanoparticles naturally coated by a biological membrane and purified magnetotactic bacteria, represents a promising alternative to overcome both the problem of coating and solubility. Magnetosomes have been shown to be safe and efficient *in vivo* MRI probes in mouse brain angiograms (13). Such biogenic particles can be genetically functionalized with peptides or proteins to confer even better selectivity to the probe (14,15). In this context, we previously demonstrated the feasibility of using genetically tailored magnetosomes to express a RGD peptide (rich in Arginine, Glycine, and Aspartic residues) recognized by several members of the superfamily of integrins present on tumor cells and involved in cancer progression (18,19). These functionalized bionanoparticles called magnetosome@RGD actively target tumor cells and blood vessels and provide unique MRI probes in brain tumour models (13,16). In addition, a therapeutic effect has been demonstrated by hyperthermia magnetic treatment (17,18), photothermal therapy (19-21), and drug delivery systems (22).

In the present study, we explored the possibility to enhance radiotherapy by using single-step produced-magnetosomes, decorated with the yellow fluorescent protein Venus and a RGD motif (magnetosomes@RGD) or with the yellow fluorescent protein Venus alone (magnetosome). We assumed that the RGD peptide would facilitate the cellular uptake of the magnetosomes, thereby increasing the dose deposited *in situ*. The potential of both forms of biogenic magnetic radiation-effect enhancing nanoparticles to increase ionizing radiation

effects was first analyzed on DNA and on two cellular models, namely colorectal cancer cells and melanoma cells known for their relative radioresistance (23) (24). We next evaluated the *in vivo* radioenhancing potential of magnetosomes@RGD after injection into mouse melanoma xenografts irradiated with photons. For radioresistant tumors surrounded by sensitive tissues, proton therapy presents a dose distribution superiority compared to other RT modalities with photons, by avoiding damage to the tissues behind the tumor. However, damages caused in front of the tumor may still remain significant and strategies to reduce radiation doses are needed. Therefore, we further explored the therapeutic efficacy of magnetosomes combined to protons. To the best of our knowledge, this study is the first to report the use of biogenic magnetic radiation-effect enhancing nanoparticles decorated with an RGD peptide as tumor radioenhancers to both X-rays and protons.

Code de champ modifié
Code de champ modifié

MATERIALS AND METHODS

Culture of magnetotactic bacteria and magnetosomes production

The bionanoparticles, magnetosomes@RGD and magnetosomes were prepared as described in Plan et al (23). Briefly, the AMB1 strain were genetically modified to biosynthesized magnetosomes@RGD and magnetosomes (Fig Supp 1A). The RGD peptide was used or not to decorate the magnetosome membrane in fusion with the yellow fluorescent protein venus and the magnetosome membrane anchor mamC (Fig Supp 1B). Western Blot experiments confirmed the insertion of MamC-Venus or MamC-Venus-RGD at the magnetosomal membrane using Anti-venus antibodies (Fig Supp 1C). Each batch of magnetosomes was systematically checked for structure by transmission electron microscopy (Fig Supp 1A) and size by Nanoparticle Tracking Analysis (Fig Supp 1B). Both genetically modified AMB-1 strains were grown in 7L bioreactor and cells from late exponential-phase culture were harvested by centrifugation (7500 g, 10 min, 4°C). The pellet (≈ 19 g per 6L) was resuspended in 100 ml of purification buffer 1 (20 mM HEPES, 1mM EDTA, 0.9% NaCl, 8% glycerol, pH 7,5 in presence of a cocktail of anti protéase). The cells were then disrupted 3 times with a French press (1000 PSI, 4°C). The tubes were left for 30 min at 4°C in contact of a magnet (MACSi-MAGtm separator, Miltenyi Biotec), resulting in magnetosomes collection. The unretained fraction was removed and the magnetosome fraction was resuspended in 45 ml of buffer. This magnetic purification step was performed 5 times with buffer 1 (without anti protease) then 5 times with buffer 2 (20 mM HEPES, 0.9% NaCl, 8% glycerol, pH 7,5). After the washing steps, the magnetosomes were resuspended in buffer 3 (20 mM HEPES, 8% glycerol, pH 7,5), at a concentration of 3 g/l of iron (ICP-AES measurement) and 100 μ L aliquots were flash-frozen in liquid nitrogen then stored at -80 °C.

Magnetite magnetosomes were biosynthesized under strict genetic control in *Magnetospirillum magneticum* strain AMB-1 (ATCC700264) (Fig Supp1A). As described in Boucher *et al* (16), the Venus fluorescent reporter was inserted in the lipid membrane by genetic manipulation. This first class of biomagnetite is simply referred to as "magnetosomes". The exact same genetic construct was used for "magnetosomes@RGD", except that, in addition to the Venus reporter, the RGD peptide was used to decorate the magnetosome membrane (Fig Supp 1B). The size of both types of particles are similar but western Blot experiments confirmed the insertion of MamC-Venus or MamC-Venus-RGD at the magnetosomal membrane using Anti-venus antibodies (Fig Supp 1C). Both genetically modified AMB-1 strains were grown in 7L bioreactor and the same procedure was used for both strains to purify the magnetosomes. Briefly, cells from late exponential-phase culture were harvested by centrifugation (7500 g, 10 min, 4°C). The pellet (≈19 g per 6L) was resuspended in 100 ml of purification buffer 1 (20 mM HEPES, 1mM EDTA, 0.9% NaCl, 8% glycerol, pH 7,5 in presence of a cocktail of anti protéase). The cells were then disrupted 3 times with a French press (1000 PSI, 4°C). The tubes were left for 30 min at 4°C in contact of a magnet (MACSi-MAGtm separator, Miltennyi Biotec), resulting in magnetosomes collection. The unretained fraction was removed and the magnetosome fraction was resuspended in 45 ml of buffer. This magnetic purification step was performed 5 times with buffer 1 (without anti protease) then 5 times with buffer 2 (20 mM HEPES, 0.9% NaCl, 8% glycerol, pH 7,5). After the washing steps, the magnetosomes were resuspended in buffer 3 (20 mM HEPES, 8% glycerol, pH 7,5), at a concentration of 3 g/l of iron (ICP-AES measurement) and 100 µL aliquots were flash-frozen in liquid nitrogen then stored at -80 °C. Each batch of magnetosomes was systematically checked for structure by transmission electron microscopy (Fig Supp 1D). 10 µl drops were deposited on grids, evaporated, and observed with a Phillips Tecnai 12 electron microscope. The images were processed with Fiji software to determine the magnetosome diameter.

Code de champ modifié

DNA preparation and radiation-induced damage quantification

pGEM-3Zf(-) plasmid DNA (3197 bp, Promega) was extracted from *E. coli* DH5 α and purified with the QIAfilter Plasmid Giga Kit (Qiagen). The DNA pellet was redissolved in TE buffer (10 mM Tris, 1 mM EDTA, pH 8) and DNA concentration was obtained by measuring its absorption at 260 nm. Solutions of DNA (100 ng) and of magnetosomes@RGD or magnetosomes (0-500 nM) were mixed just before X-rays exposure (0, 0.5, 1, 2, 3 or 5 Gy) (RX Optitop 150/40/80 HC, Siemens). DNA damages were quantified by agarose gel electrophoresis stained with SYBR[®] Gold (Invitrogen). The gels were imaged with a Luminescent Image Analyzer LAS 3000 system. Resulting images were analyzed using ImageJ software to determine the relative amounts of supercoiled, circular and linear DNA forms (25).

Cell culture

The B16F10 melanoma and the DHD/K12/TRb (PROb) colorectal cancer cells were cultured in DMEM (GIBCO, France) supplemented with 10 % heat-inactivated fetal calf serum (FCS, GIBCO) at 37 °C under a humidified atmosphere containing 5 % CO₂. Cells were passaged by using 0.05 % trypsin.

***In vitro* measurement of magnetosomes toxicity**

Five hundred DHD or B16F10 cells were plated in 96-well. After 24 h, the culture medium was replaced with 100 μ L of fresh medium or medium containing magnetosomes@RGD or magnetosomes at the indicated concentrations and incubated for 2 hours at 37 °C. After 3 washes with 1 \times PBS (pH 7.4), the treated cells were incubated for 4 days in complete medium.

Cell viability was assessed by the MTT assay using a spectrophotometer Multiskan GO microplate (Thermo Scientific).

Clonogenic cell survival assay

The radioenhanced cell kill efficacy of magnetosomes@RGD or magnetosomes to DHD and to B16F10 cells was assessed by the clonogenic assay. Different number of cells (50, 100, 300, 1000) were plated in 12-well. After 24 h, the culture medium was replaced with 1 mL of fresh medium or medium containing magnetosomes@RGD or magnetosomes at the indicated concentrations and incubated for 2 hours at 37 °C. After 3 washes with 1× PBS (pH 7.4), the treated cells were exposed to 0, 0.25, 0.5, 0.75, 1, 2 or 3 Gy of X rays (RX Optitop 150/40/80 HC, Siemens) before being incubated for 9–14 days. The colonies were fixed with methanol and stained with 0.4 % crystal violet. Finally, the plates were inspected by microscopy and the number of the colonies was counted. Each assay was made in triplicate and only colonies containing at least 50 cells were counted.

Mice

Eight-week-old Balb/c female athymic (nude) mice were obtained from Janvier (Le Genest Saint Isle, France). Animal housing and procedures were conducted according to French Agriculture Ministry guidelines and were approved by the local ethics committee.

Xenografts and treatments

Briefly, each mouse was subcutaneously injected with 5×10^5 B16F10 cells in the flank. An apparently visible tumor mass was observed 6 days after injection. At day 8, when the tumor size was about 100 mm³, the mice were randomly divided into three groups: control group (saline only), irradiation group (X rays or protons), magnetosomes@RGD/ irradiation group.

Five mice were included in each group. On day 8, mice treated with magnetosomes received either an intratumor injection (750 nmol) or an intravenous injection (4 μ mol) of magnetosomes@RGD. On day 9, mice subjected to irradiation were exposed to 5 Gy of X rays or protons. Mice were monitored after treatments. The longest (a) and shortest (b) tumor diameters (mm) were recorded and formula for an ellipsoid sphere ($0.52 \times a \times b^2$) was utilized to determine the volume of tumor. Tumors were preserved in liquid nitrogen for future studies.

Irradiation modalities

For the *in vitro* study (cells and DNA), we used the OPTITOP 150/40/80 HC x-ray tube (SIEMENS) belonging to a medical imaging table. For the *in vivo* study, mice were anesthetized and placed horizontally into a 43855F-CP160 Faxitron x-ray device (EDIMEX). To generate the same damages on cells and on mice, we adjusted the beam quality so that it be the same on both tubes: 99 kV High Voltage and 3,7 mmAl half value layer. To reach this half value layer on the faxitron's tube, we introduced a 3 mm Al aluminium filter beyond the exit window.

For *in vivo* proton therapy experiments, mice were anesthetized and placed vertically on a robotic chair device. Proton therapy was performed using a single scattering beam line device with beam energy modulation (using a range shifter and a rotating wheel placed in the beam line) in depth and beam conformation laterally using a brass collimator at the beam end. Tumors were placed within the flat portion of the modulated Bragg peak, where relative biological efficacy (RBE) of protons compared to photons is 1.1. The distal fall off, where RBE may exceed 1.1, was over the deeper part of the tumor. The dose with protons is reported in Gy RBE.

Histology/Fluorescence Images processing

Formalin-fixed, paraffin-embedded tumour sections were stained with hematoxylin/eosin for morphologic evaluation. The sections were stained with DAPI (4',6-diamidino-2-phenylindole) to visualize nuclei integrity (excitation wavelengths of 405 nm and emission wavelengths of 471 nm) and venus (YFP)-labelled magnetosomes were detected in green (excitation wavelengths of 514 nm and emission wavelengths of 542 nm). The image of Fluorescence microscopy images were acquired with a Zeiss LSM 780 microscope at $\times 63$ magnification for single field-of-view focusing on structures of interest inside the tumor.

Statistical analysis

Statistical analysis was performed using Prism (GraphPad software). Dual comparisons were made using a Student's t-test and comparisons between multiple conditions were analyzed using ANOVA. Statistical significance was set at $P < 0.05$.

RESULTS

DNA damage radioenhancement by magnetosomes

Magnetosomes@RGD and magnetosomes were prepared and characterized as described in Plan et al. (19). In order to investigate their radioenhancing effect, DNA plasmids were subjected to X rays in the presence and in the absence of both types of magnetosomes. The different forms of plasmid DNA were resolved by a 1% agarose gel electrophoresis and quantified with ImageJ software (26). Upon irradiation, the supercoiled plasmid (SC) undergoes a single-strand break (SSB) causing the molecule to adopt a circular form (CF). The native supercoiled form decrease was quantified as a function of the irradiation dose. A typical electrophoresis gel showing DNA damage after exposure to 1, 2 and to 3 Gy is presented in Figure 1A. Non-irradiated samples mainly consisted of supercoiled DNA (SC) whereas the circular form accounted for ~5%. After irradiation with doses as low as 2 Gy, the proportion of the supercoiled DNA was significantly diminished, mainly in favour of the circular form. However, 1 Gy irradiation only led to a minor change in the proportions of the SC and the CF forms, thus suggesting minor DNA damage at such dose. Therefore, the dose of 1 Gy was retained to further study the radioenhancing potential of magnetosomes. Admixing DNA with increasing concentrations of magnetosomes (5, 50 and 500 nM) led to enhanced DNA damage in response to 1 Gy X-rays, as indicated by the SC decrease concomitant with the CF increase (Figure 1B, C and D). This radioenhancing effect on DNA in the presence of magnetosomes was observed with an enhancement factor of 2.1 ± 0.3 with 50 nM ($p < 0.05$), and of 3.2 ± 0.9 ($p < 0.05$) with 500 nM magnetosomes, but remained negligible with 5 nM. Accordingly, a significant increase in the circular form was measured with 50 nM (and with 500 nM (Fig. 2D)). These results mean that in the presence of magnetosomes, only 50% and 30% of the radiation dose, respectively, is necessary to induce an equivalent damage. Similar results were obtained with magnetosomes@RGD, thus

Code de champ modifié

Code de champ modifié

Code de champ modifié

suggesting the absence of a significant impact of the RGD functionalization on the DNA radio-enhancement potential of the particles (data not shown).

Radioenhancing potential of magnetosomes on B16-F10 and DHD cells

Studies were carried out with the B16F10 (melanoma) and the DHD/K12/TRb (colorectal cancer) cells to determine the cytotoxicity of magnetosomes and magnetosomes@RGD in viability assays (Figure 2A and B). The fraction of the viable cells was determined after exposure of the cells for 2 hours to several doses of magnetosomes, ranging from 100 μ M to 1 mM, followed by cell culture for 5 days. No significant reduction in cell viability was observed after exposure of both cell types to concentrations reaching even up to 1 mM.

In order to determine whether magnetosomes and magnetosomes@RGD could radioenhance damages in melanoma and colorectal cancer cells irradiated with X-rays, the respective sensitivities of both cell lines to radiation were assessed in clonogenic assays. As shown on Figures 2C and D, the LD₅₀ (Lethal dose causing the death of 50% of cells) was obtained with 1.2 Gy in B16-F10 cells and with 0.8 Gy in DHD cells, thus indicating a lower sensitivity to radiation of the melanoma cell line to X-rays compared to the colorectal cancer cells. Radiation doses leading to approximately 20-25 % of mortality in both cell types were then chosen to assess the potential enhancement factor of magnetosomes, precisely 0.75 Gy for B16F10 cells and 0.25 Gy for DHD cells. The effect of pretreating the cells for 2 hours with 200 μ M magnetosomes or magnetosomes@RGD before irradiation was tested. Figures 2E and 2F show in both cells types a moderate enhancement factor with magnetosomes/ X-rays compared to X-rays alone. Interestingly, this enhancing effect was much more pronounced with the functionalized magnetoparticles. Indeed, magnetosomes@RGD could reduce the cell survival fraction from 81% to 50% for the B16F10 cells (Figure 2E) and from 75% to 28% for the DHD

cells (Figure 2F), thus suggesting the ability of the membrane-anchored RGD motif to promote the binding and the internalization of the magnetoparticles by both targeted cells.

Assessment of radioenhancing potential of magnetosomes@RGD *in vivo*

Cellular damage radioenhancement observed here for magnetosomes@RGD together with their high efficient internalization previously observed in tumor cells (18-21) prompted us to investigate their radioenhancing potential in a tumour xenograft model. The B16 xenograft model was chosen based on the observation that the B16-F10 melanoma cells proved to be more resistant against radiation *in vitro* than the colorectal DHD cells. B16 tumours were generated on the flank of Balb/c mice and allowed to grow for one week. At day 8 post-induction with melanoma cells, mice developed tumours with an average volume of 50 mm³, at which point, animals were randomly assigned to one of 2 treatment groups: saline (control) or magnetosomes@RGD, delivered by 3 intratumoral injections. At day 9, half of the tumors in the saline- and in the magnetosome-treated groups were administered a single dose of 5 Gy X-rays. Tumor progression was then measured over time and compared between the four groups: saline, magnetosomes@RGD, X-rays, magnetosomes@RGD/ X-rays.

Figure 3A shows that control xenografts grew up to approximately 600 mm³ within 17 days after implantation. Histologic analysis of the tumours shows highly proliferative cancer cells (Figure 4A). Treatment with magnetosomes@RGD alone had minimal impact on tumour growth and the tumour mass failed to show any remarkable change compared to the untreated group. The 5Gy X-rays treatment by day 9 significantly impaired tumor progression resulting in a 29% reduction in the tumor volume by day 17 (425 mm³ in the X ray group vs 620 mm³, in the control group, p= 0.03). In agreement with the radioenhancing effects observed *in vitro*, the combination of magnetosomes / 5Gy X-rays attenuated tumor growth by nearly 50% over radiation alone (217 mm³ in the magnetosomes@RGD /X-ray group vs 425 mm³ in the X-ray

group, $p=0.039$), leading to an overall 65% decrease in lesion size compared to control xenografts. The most remarkable observation on the lesions treated with magnetosomes@RGD/X-rays was the presence of large areas of necrosis that extended deep into the core of the tumours, whereas 5-Gy irradiated tumors rarely demonstrated necrosis at necropsy (Figure 4C and D).

Upon observation of the radioenhancing effects of combining RGD-functionalized magnetoparticles with X-rays, we next explored the ability of the nanomaterial to enhance the radiation effect of proton therapy using the same melanoma xenograft model. As shown on Figure 3B, a single 5 Gy RBE irradiation with protons led to a 37% reduction in tumor growth by day 17 (392 mm^3 in the proton group vs 620 mm^3 , in the control group, $p=0.027$). However, this reduction was not statistically significant compared to that induced by 5 Gy X-rays. Tumour development was further decreased by 40% when combined treatments magnetosomes@RGD/protons were administered to mice (Figure 3B), thus leading to lesions 77% smaller than the untreated xenografts (139 mm^3 in the magnetosomes@RGD / protons group vs 620 mm^3 , in the control group, $p=0.008$). This enhancement effect of the magnetosomes upon proton therapy was significantly superior when measured by day 17 compared to that measured upon X-rays ($p=0.04$) and consistently correlated with the extent of histologic tumor necrosis post-irradiation in the treated lesions (Figure 4F).

We next studied whether the occurrence of necrosis was associated with the presence of magnetosomes@RGD within melanoma biopsies isolated at necropsy. Necrosis reflected by the loss of DNA integrity within the tumour cells was visualized by DAPI staining revealing cell nuclei in blue. The localization of magnetosomes@RGD within melanoma tumours was assessed by confocal immunofluorescence analysis of the green Venus protein (Figure 5). As expected, control melanoma biopsies exhibited intact nuclei (Figure 5A), whereas irradiated lesions showed partially altered DNA integrity within nuclei (Figure 5B). Enrichment of lesions

with magnetosomes@RGD led to marked DNA fragmentation reflecting the histologic necrosis observed in the treated tumours on the trans images (Figure 5C). Such necrotic patterns were associated with the presence of numerous Venus-labelled-magnetoparticles. Interestingly, the magnetosomes@RGD were still detectable at necropsy 9 days after injection into tumours. Altogether, these data suggest that the accumulated magnetosomes@RGD in the tumour region significantly boosted the efficacy of radiotherapy and delayed tumour growth.

DISCUSSION

Magnetic nanoparticles can induce enhanced radiation effects and can be functionalized (7-9) by adding a coating shell on their surface. Specific shell coating stabilizes the nanoparticles and favors interactions with biological systems, while protecting the surrounding environment from radiation-induced oxidation. However, synthesis of functional groups to accommodate may be complex. An alternative approach to the complex conventional synthetic routes is to exploit the controlled formation of stable and well-ordered solid inorganic compounds by biological systems, such as magnetotactic bacteria. Recently, several studies including those from our group have demonstrated the great properties of magnetosomes, biogenic magnetoparticles naturally coated by a biological membrane, for various biomedical applications. Thanks to their bio-magnetic properties, the magnetosome diagnostic potential have been revealed in MRI field (13) (16) and a therapeutic effect has been demonstrated by hyperthermia magnetic treatment (17,18), photothermal therapy (19-21), and drug delivery systems (22).

In the present study, we explored the radiation enhancement potential of magnetosomes genetically modified to express RGD motifs capable of actively targeting tumor cells and angiogenic blood vessels. Our *in vitro* data show that native magnetosomes and magnetosomes@RGD are equally efficient to promote the damaging action of X-rays directly on DNA. On cancer cells however, cellular damage radioenhancement observed for magnetosomes@RGD was greater than that of unlabeled particles. Our quantitative measures revealed that magnetosomes@RGD could increase the mortality by 2.5 fold in melanoma cells and by 2.9 fold in colorectal cancer cells, with irradiating doses set at 0.75 and at 0.25 Gy, respectively. The fact that lower mortality is obtained in melanoma cells despite the use of higher radiation doses compared to colorectal cancer cells is consistent with the higher

radioresistance of the melanoma cells. Of note, a short incubation time of the cancer cells with both types of magnetosomes was deliberately chosen in order to clearly assess the potential impact of the RGD functionalization at the magnetosome surface on the cellular uptake. This result is in accordance with our previous observations showing that internalization of control magnetosomes on cancer cells is not optimal within 2 hours and can be markedly increased by lengthening the incubation time up to 24 hours (16). However, the RGD-mediated high efficient internalization of magnetoparticles previously observed by our group in tumor cells still remained despite longer incubation times. In terms of mechanism, DNA damage is commonly considered as the cause of radiation-induced cell death (27,28). Consistently, nanoparticles have been proposed to enhance ionizing radiation effects through an amplification of this DNA damage. However, many *in vitro* studies indicated that the radiation-effect enhancing nanoparticles located in the cell cytoplasm also seem to amplify cell killing without entering the nucleus (29-34), simply by generating electron showers capable of spreading as far as several micrometers (35).

Encouraged by the *in vitro* performance of magnetosomes@RGD with X-rays, we further explored the potential of the combined therapy in B16 xenografts. As a monotherapy administered on day 9 after tumor implantation into mice, 5 Gy X-rays were able to reduce tumor growth by 29 %, indicating the tumor-inhibiting efficacy of radiation. The enrichment of tumours with magnetosomes@RGD prior to radiotherapy led to a much more effective tumor growth inhibition compared to radiation alone, lesions being reduced by 65 % in volume. In addition, the treated lesions featured much larger necrotic areas colocalizing with the accumulated magnetoparticles thus confirming the ability of RGD-decorated magnetosomes to boost the killing efficacy of ionizing radiations. Interestingly, we observed that the magnetosomes@RGD were still detectable at necropsy 9 days after injection. Considering that the 65% reduction in tumor size was obtained after a single irradiation, it is tempting to

speculate that much more impressive tumour inhibition could be observed with repeated X-ray treatments.

Beyond conventional radiotherapy, nanomedicine have also been envisaged to optimize proton therapy. Indeed, targeting tumours with protons enables to spare healthy tissue sited behind the tumour region due to the physical superiority of protons represented by their abrupt energy loss and finite dose deposition at the end of their predefined range. However, the radiation dose received by tissues in front of the tumor still needs to be reduced, especially when tumors are adjacent to critical structures such as in brain or head and neck tumours. Based on the convincing results obtained when combining magnetosomes@RGD to X-rays, we further investigated the ability of magnetoparticles to amplify the killing efficacy of protons using the similar melanoma model. Although, 5 Gy RBE protons similarly reduced tumor growth compared to 5 Gy X-rays, melanoma tumours appeared clearly smaller with the magnetosome-proton therapy compared to the same combination with X-rays. These data suggest a higher radioenhancing potential of the magnetosomes upon irradiation with protons rather than photons. In addition to the 1.1 radiobiological efficacy of protons compared to photons, such differences might be explained by different nuclear reactions of the magnetite crystal under distinct radiations types. Naturally occurring iron (^{56}Fe) consists of four stable isotopes, among which ^{56}Fe accounts for 91%. Whereas excitation of ^{56}Fe by photons follows a (p, n) reaction, protons can produce a $^{56}\text{Fe}(p,2n)^{55}\text{Co}$ reaction generating twice more secondary electrons compared to X rays, and therefore potentially more damaging effects within cells (36). Such hypothesis is consistent with the enhanced extent of necrosis visualized within magnetosomes@RGD-treated melanoma tumors irradiated with protons compared to photons.

In conclusion, our work provides the first evidence of the radioenhancing potential of magnetosomes@RGD in conventional radiotherapy and proton therapy and pave the way

to promising investigations using systemic administration of the particles. The combined features including simple preparation, good biocompatibility, active cancer cell targeting property, strong radioenhancing effect and potential PET imaging capability under proton therapy strengthen the interest of developing biogenic magnetoparticles for multimodal nanomedicine for cancer therapy.

FIGURE LEGENDS

Figure 1: DNA damage radioenhanced by magnetosomes and magnetosomes@RGD. (A) Typical agarose gel electrophoresis showing DNA damage after exposure to 1, 2 and to 3 Gy X rays. Non-irradiated DNA mainly consists of supercoiled DNA (SC). Upon irradiation, the supercoiled plasmid (SC) undergoes a single-strand break (SSB) causing the molecule to adopt a circular form (CF). MM: Mass marker. (B) Influence of the magnetosome concentration on the loss of the native supercoiled DNA induced by 1Gy X-rays. Representative electrophoresis gels showing the loss of the SC form and the increase in the CF form of DNA irradiated in the presence of increasing concentrations of magnetosomes (upper panel) or magnetosomes@RGD (lower panel). Quantification of the loss of native supercoiled DNA (C) and of the increase in the circular form DNA (D) versus magnetosomes concentrations. The data presented are the mean \pm SEM of triplicates and are representative of three independent experiments. * $p < 0.05$; ** $p < 0.01$.

Figure 2: Radioenhancement potential of magnetosomes and magnetosomes@RGD on B16F10 melanoma and DHD colorectal carcinoma cells. Cytotoxicity assays of B16F10 (A) and DHD (B) cells in the presence of increasing concentrations of magnetosomes or magnetosomes@RGD. Cell survival rate of B16F10 (C) and DHD (D) cells irradiated by X-rays at the indicated doses. Cell viability of B16F10 (E) and DHD (F) cells assessed in clonogenic assays on cancer cells pretreated for 2 hours with 200 μ M magnetosomes or magnetosomes@RGD prior to X-rays at the indicated dose. The data presented are the mean \pm SEM of triplicates and are representative of three independent experiments. * $p < 0.05$; ** $p < 0.01$.

Figure 3: Assessment of radioenhancing potential of magnetosomes@RGD in vivo. Melanoma xenograft-bearing mice were subjected to (A) X-rays (5 Gy) or (B) protons (5 Gy).

Tumor development was monitored over time in mice untreated (filled circles) or treated with either magnetosomes@RGD alone (open circles), or with 5 Gy X rays (filled squares), or with a combination of magnetosomes@RGD / X rays (filled triangles), with 5 Gy protons (open squares), or with a combination of magnetosomes@RGD / protons (open triangles). (n = 5 mice per condition). * p < 0.05; ** p < 0.01.

Figure 4: Histology of B16 tumors after treatment with radiotherapy combined or not with magnetosomes@RGD. Tumor histology was compared on sections (10X magnification) of lesions from B16-challenged mice either untreated (A, C, E), or treated with RGD-V-AMB1 magnetosomes (B, D, F) before receiving radiotherapy with X-rays (C, D) or with protons (E, F). *N*=area of necrosis in a liver tumor.

Figure 5: Fluorescent analyses of B16 tumors after treatment with radiotherapy combined or not with magnetosomes@RGD. Confocal microscopy on untreated (A), X-rays treated (B) or magnetosome@RDG injection and X-rays treated (C) tumors sections. The nuclei were visualized in blue after DAPI staining and the magnetosome@RGD were detectable in yellow tanks to the venus protein. Transmission acquisition with nucleus staining and magnetosomes@RGD are shown in the overlay images.

Figure S1: Synthesis and characterization of magnetosomes. (A) Representative TEM image of *Magnetospirillum magneticum* (AMB-1) and isolated magnetosomes. (B) Size distribution of magnetosomes suspension performed using Nanoparticle Tracking Analyse (NTA), indicating for both magnetosome@RGD (upper panel) and magnetosomes (bottom panel) a crystal size of 50 nm surrounded by a bilipidic bilayer of 2X 12nm. (C) The correct functionalization was verified by (a) SDS-PAGE gel (10% acrylamide) with 5 µg of magnetosomal proteins per lane stained with Coomassie blue (lane 1: Magnetosomes@RGD 43.7 kDa, lane 2: Magnetosomes 42.5 kDa), and (b) Western blot with 1µg of magnetosomal

protein per lane probed with Living Colors® A.v. Monoclonal Antibody (JL-8) against venus protein (lane 1: Magnetosomes@RGD 43.7 kDa, lane 2: Magnetosomes 42.5 kDa).

Abbreviations

RT

MTS

RGD: rich in Arginine, Glycine, and Aspartic residues

MRI:

AMBI:

MTT:

SYBR:

AND:

Gy:

DAPI:

YFP

ACKNOWLEDGEMENTS

This work was supported by INSERM, the French National Research Agency (ANR) and by a grant from CEA/PTTox. We thank Colette Ricort for assistance in preparing the manuscript.

We thank the IRCAN Animal Core Facility for providing access to their equipment. The authors also thank the Zoom platform (Biosciences and biotechnology Institute of Aix-Marseille) for the access to the Zeiss LSM780 microscope and Pierre Richaud for ICP analysis. Michel Péan and Nicolas Ginet are acknowledged for fruitful discussions on biomedical applications of magnetosomes.

Competing interests:

All authors declare that no competing interest exists.

REFERENCES

1. Jemal A, Bray F, Center MM, Ferlay J, Ward E, Forman D. Global cancer statistics. *CA Cancer J Clin.* 2011;61:69-90.
2. Maier-Hauff K, Ulrich F, Nestler D, et al. Efficacy and safety of intratumoral thermotherapy using magnetic iron-oxide nanoparticles combined with external beam radiotherapy on patients with recurrent glioblastoma multiforme. *J Neurooncol.* 2011;103:317-324.
3. Bradbury MS, Phillips E, Montero PH, et al. Clinically-translated silica nanoparticles as dual-modality cancer-targeted probes for image-guided surgery and interventions. *Integr Biol (Camb).* 2013;5:74-86.
4. Hainfeld JF, Dilmanian FA, Slatkin DN, Smilowitz HM. Radiotherapy enhancement with gold nanoparticles. *J Pharm Pharmacol.* 2008;60:977-985.
5. McMahon SJ, Hyland WB, Muir MF, et al. Biological consequences of nanoscale energy deposition near irradiated heavy atom nanoparticles. *Sci Rep.* 2011;1:18.
6. Kainz K, Chen GP, Chang YW, et al. A planning and delivery study of a rotational IMRT technique with burst delivery. *Med Phys.* 2011;38:5104-5118.
7. Michel SC, Keller TM, Frohlich JM, et al. Preoperative breast cancer staging: MR imaging of the axilla with ultrasmall superparamagnetic iron oxide enhancement. *Radiology.* 2002;225:527-536.
8. Enochs WS, Harsh G, Hochberg F, Weissleder R. Improved delineation of human brain tumors on MR images using a long-circulating, superparamagnetic iron oxide agent. *J Magn Reson Imaging.* 1999;9:228-232.
9. Semelka RC, Helmlinger TK. Contrast agents for MR imaging of the liver. *Radiology.* 2001;218:27-38.
10. Bakhtiary Z, Saei AA, Hajipour MJ, Raoufi M, Vermesh O, Mahmoudi M. Targeted superparamagnetic iron oxide nanoparticles for early detection of cancer: Possibilities and challenges. *Nanomedicine.* 2016;12:287-307.
11. Sharifi S, Seyednejad H, Laurent S, Atyabi F, Saei AA, Mahmoudi M. Superparamagnetic iron oxide nanoparticles for in vivo molecular and cellular imaging. *Contrast Media Mol Imaging.* 2015;10:329-355.
12. Veisheh O, Gunn JW, Zhang M. Design and fabrication of magnetic nanoparticles for targeted drug delivery and imaging. *Adv Drug Deliv Rev.* 2010;62:284-304.

13. Meriaux S, Boucher M, Marty B, et al. Magnetosomes, biogenic magnetic nanomaterials for brain molecular imaging with 17.2 T MRI scanner. *Adv Healthc Mater.* 2015;4:1076-1083.
14. Xie J, Chen K, Chen X. Production, Modification and Bio-Applications of Magnetic Nanoparticles Gestated by Magnetotactic Bacteria. *Nano Res.* 2009;2:261-278.
15. Mathuriya AS. Magnetotactic bacteria: nanodrivers of the future. *Crit Rev Biotechnol.* 2016;36:788-802.
16. Boucher M, Geffroy F, Preveral S, et al. Genetically tailored magnetosomes used as MRI probe for molecular imaging of brain tumor. *Biomaterials.* 2017;121:167-178.
17. Alphantery E, Idbaih A, Adam C, et al. Development of non-pyrogenic magnetosome minerals coated with poly-L-lysine leading to full disappearance of intracranial U87-Luc glioblastoma in 100% of treated mice using magnetic hyperthermia. *Biomaterials.* 2017;141:210-222.
18. Mannucci S, Ghin L, Conti G, et al. Magnetic nanoparticles from *Magnetospirillum gryphiswaldense* increase the efficacy of thermotherapy in a model of colon carcinoma. *PLoS One.* 2014;9:e108959.
19. Plan Sangnier A, Preveral S, Curcio A, et al. Targeted thermal therapy with genetically engineered magnetite magnetosomes@RGD: Photothermia is far more efficient than magnetic hyperthermia. *J Control Release.* 2018;279:271-281.
20. Chen C, Wang S, Li L, et al. Bacterial magnetic nanoparticles for photothermal therapy of cancer under the guidance of MRI. *Biomaterials.* 2016;104:352-360.
21. Mondal G, Barui S, Chaudhuri A. The relationship between the cyclic-RGDfK ligand and alphavbeta3 integrin receptor. *Biomaterials.* 2013;34:6249-6260.
22. Wang X, Wang JG, Geng YY, et al. An enhanced anti-tumor effect of apoptin-cecropin B on human hepatoma cells by using bacterial magnetic particle gene delivery system. *Biochem Biophys Res Commun.* 2018;496:719-725.
23. Jingu K, Matsushita H, Yamamoto T, et al. Stereotactic Radiotherapy for Pulmonary Oligometastases From Colorectal Cancer: A Systematic Review and Meta-Analysis. *Technol Cancer Res Treat.* 2018;17:1533033818794936.
24. Buontempo F, Orsini E, Zironi I, et al. Enhancing radiosensitivity of melanoma cells through very high dose rate pulses released by a plasma focus device. *PLoS One.* 2018;13:e0199312.

25. Schneider CA, Rasband WS, Eliceiri KW. NIH Image to ImageJ: 25 years of image analysis. *Nat Methods*. 2012;9:671-675.
26. Brun E, Sanche L, Sicard-Roselli C. Parameters governing gold nanoparticle X-ray radiosensitization of DNA in solution. *Colloids Surf B Biointerfaces*. 2009;72:128-134.
27. Kassis AI, Adelstein SJ. Radiobiologic principles in radionuclide therapy. *J Nucl Med*. 2005;46 Suppl 1:4S-12S.
28. Belli M, Sapora O, Tabocchini MA. Molecular targets in cellular response to ionizing radiation and implications in space radiation protection. *J Radiat Res*. 2002;43 Suppl:S13-19.
29. Chang MY, Shiau AL, Chen YH, Chang CJ, Chen HH, Wu CL. Increased apoptotic potential and dose-enhancing effect of gold nanoparticles in combination with single-dose clinical electron beams on tumor-bearing mice. *Cancer Sci*. 2008;99:1479-1484.
30. Zhang X, Xing JZ, Chen J, et al. Enhanced radiation sensitivity in prostate cancer by gold-nanoparticles. *Clin Invest Med*. 2008;31:E160-167.
31. Porcel E, Tillement O, Lux F, et al. Gadolinium-based nanoparticles to improve the hadrontherapy performances. *Nanomedicine*. 2014;10:1601-1608.
32. Rima W, Sancey L, Aloy MT, et al. Internalization pathways into cancer cells of gadolinium-based radiosensitizing nanoparticles. *Biomaterials*. 2013;34:181-195.
33. Usami N, Furusawa Y, Kobayashi K, et al. Mammalian cells loaded with platinum-containing molecules are sensitized to fast atomic ions. *Int J Radiat Biol*. 2008;84:603-611.
34. Kong T, Zeng J, Wang X, et al. Enhancement of radiation cytotoxicity in breast-cancer cells by localized attachment of gold nanoparticles. *Small*. 2008;4:1537-1543.
35. Leung MK, Chow JC, Chithrani BD, Lee MJ, Oms B, Jaffray DA. Irradiation of gold nanoparticles by x-rays: Monte Carlo simulation of dose enhancements and the spatial properties of the secondary electrons production. *Med Phys*. 2011;38:624-631.
36. Graves SA, Ellison PA, Barnhart TE, et al. Nuclear excitation functions of proton-induced reactions ($E_p = 35 - 90$ MeV) from Fe, Cu, and Al. *Nucl Instrum Methods Phys Res B*. 2016;386:44-53.

Graphical abstract

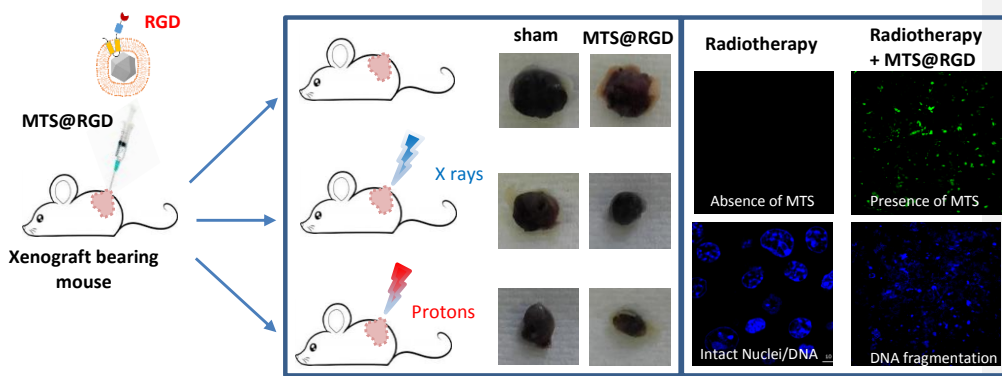
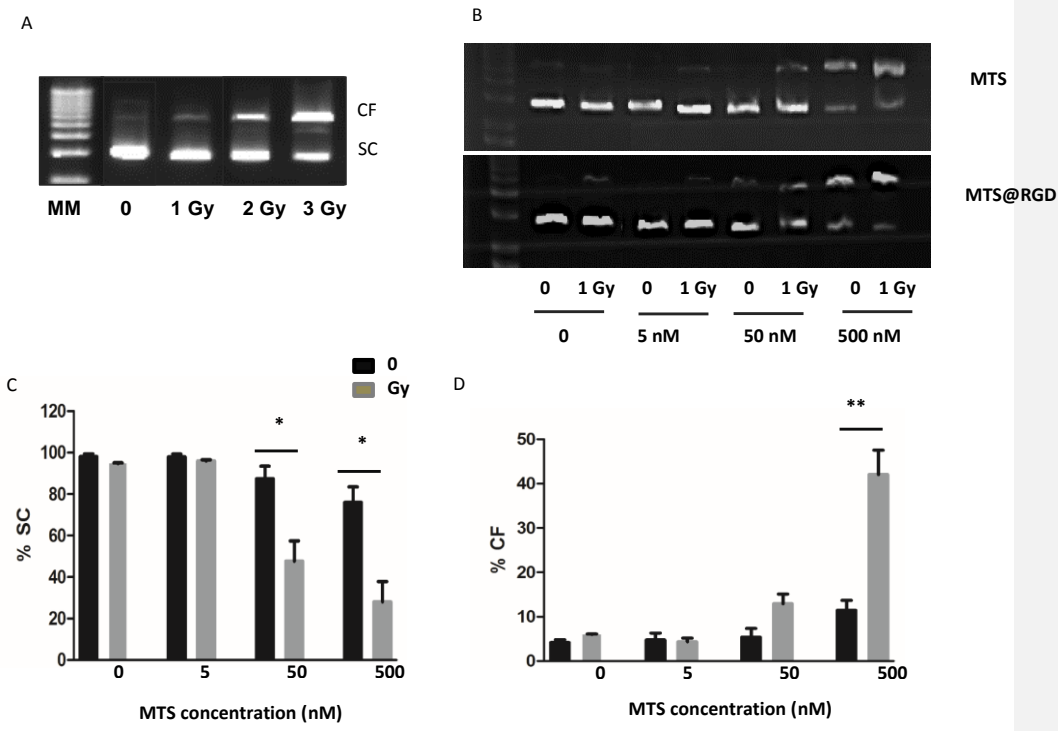
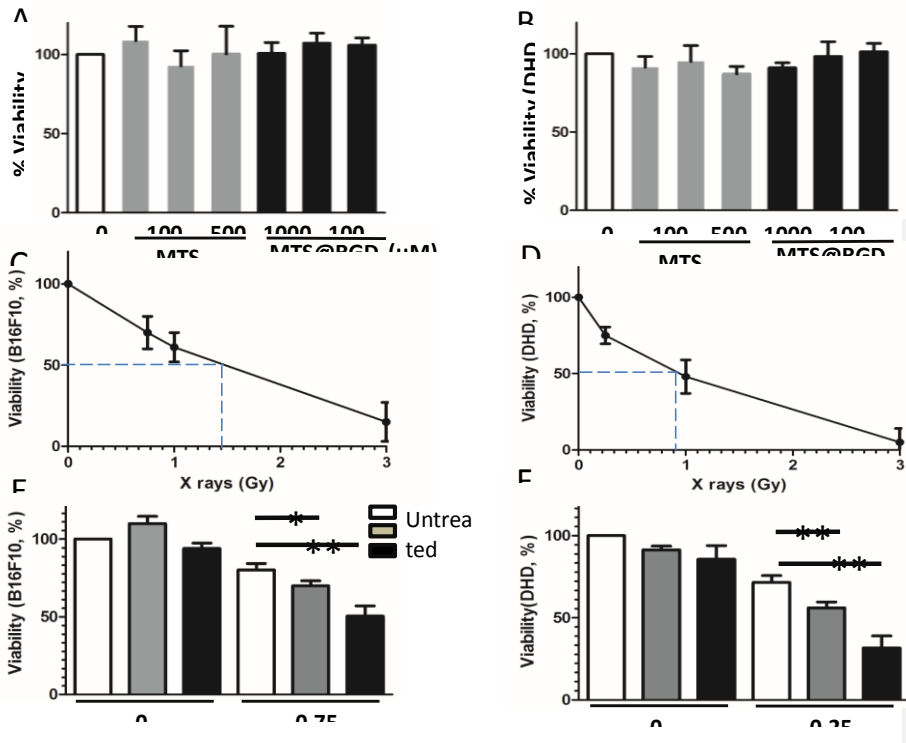


Figure 1



Figure



Figur

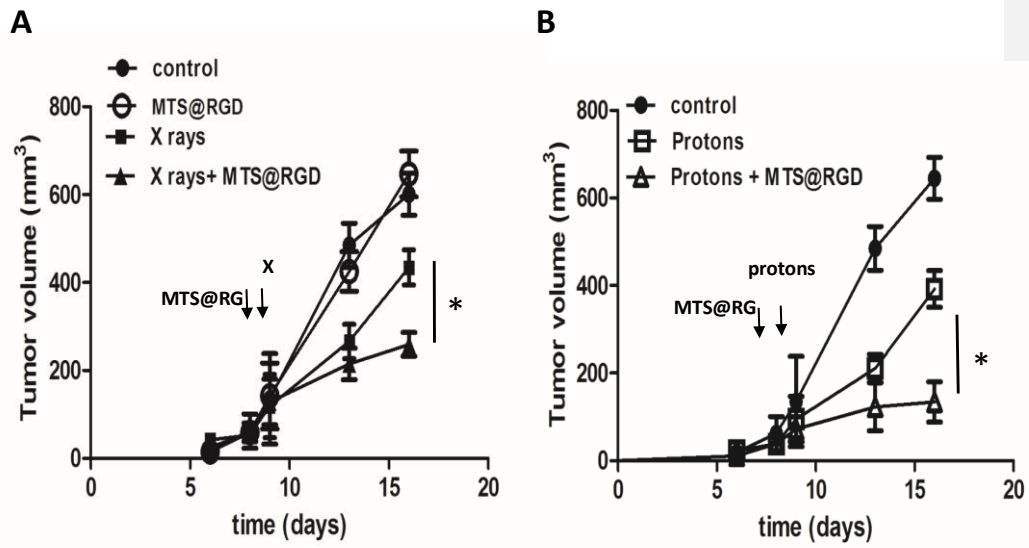
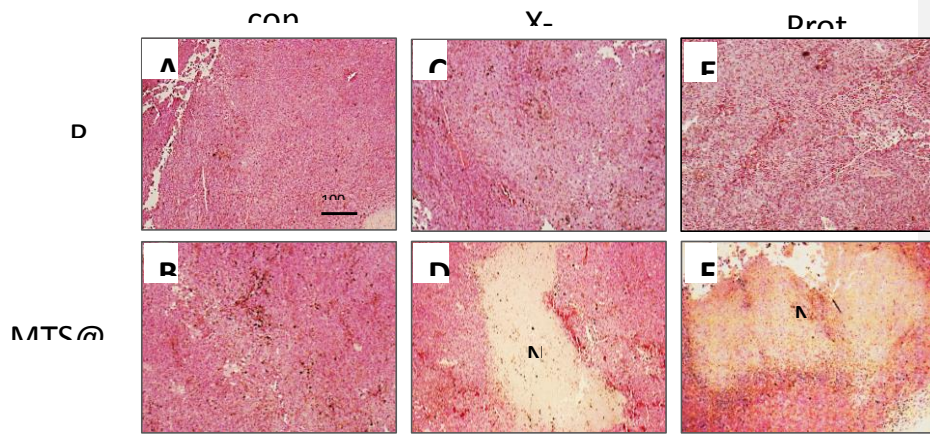
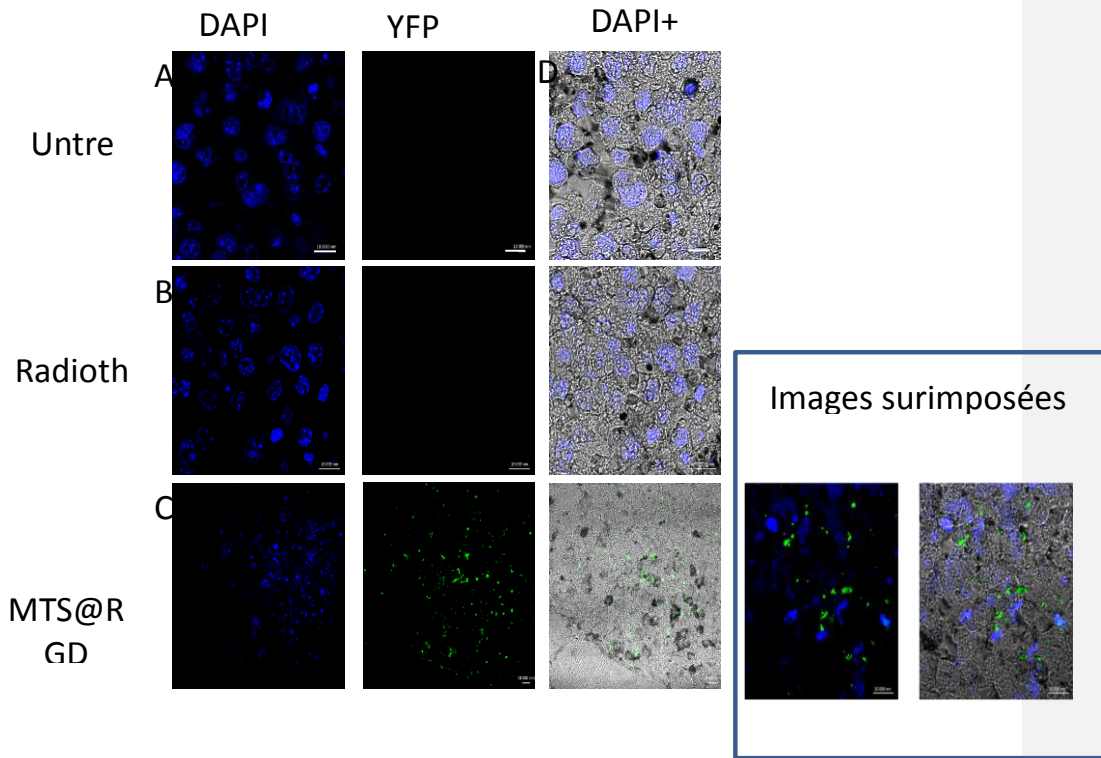


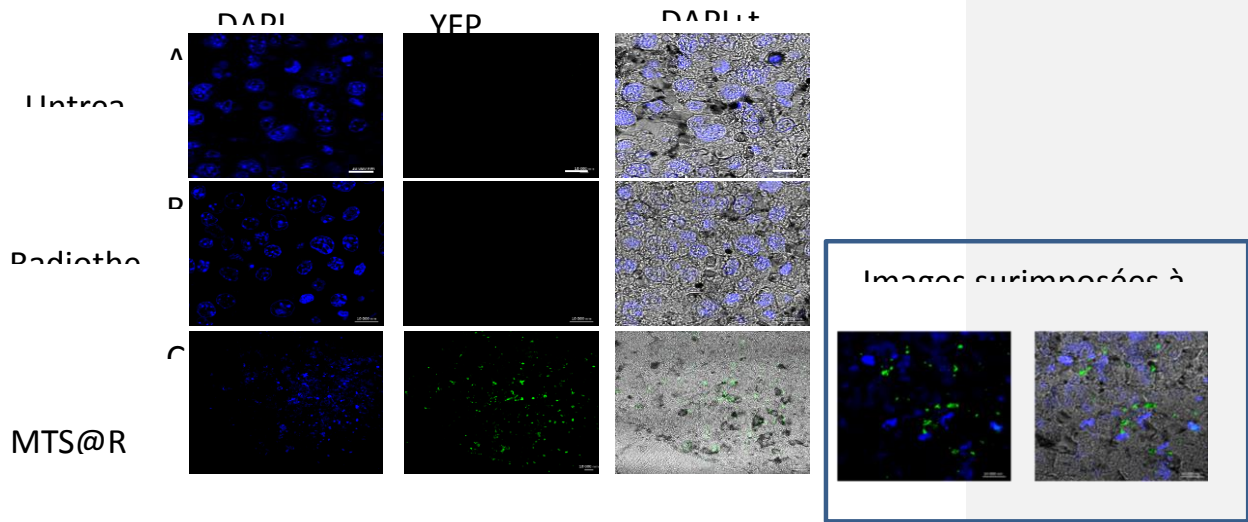
Fig 11



Fig



Figure



|